

Chapter 2

Friction, Cohesion, and Slope Stability

Every solid or liquid mass on Earth is influenced by gravity. A mass of soil or rock remains stable if the gravity force is counterbalanced by the reaction forces exerted by the adjacent bodies and the terrain. Rock masses and soils on the surface of the Earth appear steady at first sight. However, this impression is often deceiving, as the masses may slowly creep, terminating with a sudden collapse. Natural buttressing of a potential landslide may be removed or weakened, causing portions of the mass to fall. Change in stability conditions may be consequent to a variety of causes such as river undercutting or ice melting. Earthquakes can instantly change the local force equilibrium, anticipating the fall. The process of mountain building continuously overloads rock masses with renewed stress throughout time scales of several million years. Newly produced deposits may also become unstable. For example, volcanic eruptions deposit enormous amounts of pyroclastic materials, which may subsequently be mobilized by rain.

A landslide starts as consequence of terrain instability, and for this reason it is important in geotechnical practice to ascertain the stability conditions of soils or rocks. Owing to the significance in the prevention of disasters, slope stability has been the subject of much effort. There exist numerous numerical models, textbooks, and computer programs for assessing the stability on different kinds of terrain. Here the problems of instability and the initiation phase of a landslide are very briefly considered, limiting ourselves to only a few basic concepts.

The chapter starts with the basic laws of friction and cohesion, of fundamental importance not only for the problems of slope stability, but also for the dynamics of landslides.

The figure shows parallel tension cracks in soil, indicative of instability. The whole area is subject to creep, which may culminate in a catastrophic landslide. The barren surface visible in the background is part of the detachment niche of a landslide that on June 20, 1990, cost the life of at least 170 people. Most of the bodies were never found. Fatalak (Iran), April 2003.



2.1 Friction and Cohesion

2.1.1 Normal and Shear Stresses

Consider an object like a book resting on a plane inclined with angle β . Because we assume the book to be static, according to the laws of dynamics the gravity force must be counterbalanced by the reaction force exerted by the table. The gravity force can be decomposed into the components normal F_{\perp} and parallel F_{\parallel} to the plane: $F_{\perp} = Mg \cos \beta$ and $F_{\parallel} = Mg \sin \beta$. The component of gravity F_{\parallel} is equal and opposite to the reaction force, so that there is no net force perpendicular to the plane (Fig. 2.1). The force balance parallel to the plane is more complex and requires introducing the friction force (\rightarrow Sect. 2.2).

We first define normal stress σ and shear stress τ the force, divided by the area S of the surface in contact, respectively, normal and parallel to the plane. Expressing the magnitude of the weight force as $\rho g D' S$, we can write

$$\begin{aligned}\sigma &= \frac{F_{\perp}}{S} = \frac{\rho g D' S \cos \beta}{S} = \rho g D' \cos \beta = \rho g D \cos^2 \beta \\ \tau &= \frac{F_{\parallel}}{S} = \frac{\rho g D' S \sin \beta}{S} = \rho g D' \sin \beta = \rho g D \sin \beta \cos \beta.\end{aligned}\tag{2.1}$$

where $D' = D \cos \beta$ is the thickness of the object and D is the vertical projection of the thickness (Fig. 2.1). The stress is measured in pascals (Pa).

2.1.2 Friction

2.1.2.1 Basic Laws of Friction

The friction force is universally present in everyday life. The very actions of walking, running, or driving a car are possible because friction acts between the surfaces of solid bodies. A pond of oil on the road reduces the friction between the car tires and the road, causing a dangerous loss of grip. Friction is perhaps better known for its negative implications: parasitic resistance between different parts

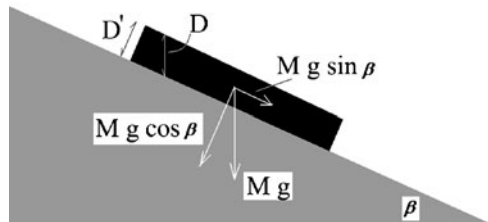


Fig. 2.1 Elementary geometrical elements for the identification of normal and shear stress

of engines, overheating of joints and machines, wear, and loss of efficiency in industrial processes.

The physics of friction was explored for the first time by Leonardo da Vinci (1452–1519). Leonardo established that the friction force is proportional to the total weight but is independent of the mass distribution. However, like many other discoveries of the renaissance genius, these studies on friction were lost for centuries. At the end of the seventeenth century, Guillaume Amontons (French inventor and physicist, 1663–1705) rediscovered the same principles, and further noticed that, at least for the materials he experimented, the friction force was about one third of the load. Nearly one century later another Frenchman, Charles-Augustine de Coulomb (1736–1806), famous for his studies on electricity, attempted a physical explanation of the laws of friction described empirically by Amontons.

To study the friction forces, the experimenter applies a force parallel to a horizontal plane as shown in Fig. 2.2. The force F_A in correspondence of which the body begins to move is the friction force.

In modern terminology, the properties of the friction force as found by Leonardo da Vinci, Amontons, and Coulomb, can be stated as follows:

1. The friction force is independent of the contact area between the two surfaces. For example, if the body is shaped as a parallelepiped with different faces, the friction force is independent on which face it rests.
2. The friction force F_A is found to be proportional to the body weight $P = Mg$, where M is the body mass. The ratio $\mu = F_A/P$ between the two forces is thus independent of the mass and of the gravity field; it is called the static friction coefficient. In shorthand,

$$F_A = \mu P. \quad (2.2)$$

3. Typically, the magnitude of the friction force is comparable for materials of similar properties. For metals it is about one third of the weight, and for rocks it is about one half of the weight (which means friction coefficients of $1/3$ and $1/2$, respectively).
4. As stated earlier, a body remains static if the applied tangential force is smaller than the friction force. Let a horizontal force F'_A slightly exceeding the friction force be applied to the center of mass of the body. The body starts moving along

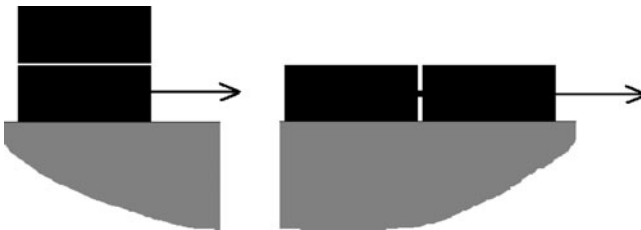


Fig. 2.2 Whether the weights are on top of each other or besides, the friction force is the same

the direction of the applied force, and with constant acceleration given by Newton's law of dynamics $a = (F'_A - F_A)/M$. Hence, when the body is moving, the friction force is collinear to the tangential force but has opposite direction.

5. At a closer inspection, point 4 results to be an oversimplification. This is because the friction force necessary to commence sliding is greater than that measured during sliding. Distinguishing a static from a dynamic friction force $F_{A,DYN}$, one should properly write $a = (F'_A - F_{A,DYN})/M$ where $F_{A,DYN} < F_A$ is the dynamic friction force. Experiments, however, show that the static and dynamic frictions do not differ much, and for practical purposes this difference may be neglected, or $F_{A,DYN} \approx F_A$. Dealing with landslides, many effects like the presence of pore water or the variability of rock behavior will influence the friction coefficient in a more substantial manner. The description in terms of two different coefficients is an oversimplification, anyhow. A full analysis would require considering the whole process from the static condition to full sliding. In fact, the friction coefficient decreases continuously as a function of the time of contact between the two surfaces, reaching a constant value after fractions of a second.
6. The friction force is only weakly dependent on the velocity. For many practical purposes it can be considered as independent of it.

2.1.2.2 Inclined Plane

It has been shown (\leftarrow Sect. 2.1) that the gravity force parallel and perpendicular to an inclined plane are, respectively, $Mg \sin \beta$ and $Mg \cos \beta$. From point (2) it follows that in the presence of friction, the force necessary to set a body in motion is $Mg\mu \cos \beta$. The condition of instability becomes $Mg \sin \beta > Mg\mu \cos \beta$ from which it follows $\tan \beta > \mu$. Thus, increasing the inclination angle the body starts to glide once a threshold angle ϕ is reached. This angle is called the friction angle. Equating the friction coefficient to the ratio between friction and normal force, it is obtained that

$$\mu = \frac{Mg \sin \phi}{Mg \cos \phi} = \tan \phi \quad (2.3)$$

showing that the friction coefficient is the tangent of the friction angle.

2.1.2.3 Microscopic Interpretation of Friction

In the following discussion we consider in particular rock for our analysis, though many of the concepts apply to other kinds of materials as well, such as metals. Even if the surface of polished rock appears smooth, at the microscopic level it reveals an irregular outline. Thus, the regions of contact between the surfaces of two bodies are irregularly distributed; as a consequence the effective surface of contact is much smaller than the geometric contact area of the two bodies.

According to the adhesion theory of friction, two solid bodies in contact yield off in correspondence of the areas where asperities come in contact, a little like loaded spring. Partial welding takes place around these areas, forming so-called *junctions*. Adhesion is explained as the resistance due to microscopic welding around asperities. We can anticipate a proportionality relationship between the effective area of contact A_r and the loading pressure P in the following way

$$\frac{P}{p} = A_r \quad (2.4)$$

where a material property p called the *penetration hardness* accounts for the strength of the material. It represents the efficiency of indentation between the two solid surfaces: a high value indicates a small deformation at the junctions. The penetration hardness is linked to the yield stress of the material. For example, for metals the hardness is about three times the yield stress (Rabinowicz 1995).

So far, we have examined the behavior of the two bodies during compression. To test the adhesion theory in predicting the properties of friction force, we need to consider the role of shear force applied between the two surfaces. For slippage to occur, the shear strength of the rocks must be overcome in correspondence of the junctions. Calling s the shear strength of the material, the friction force F is predicted by the theory to be

$$F = sA_r. \quad (2.5)$$

From (2.4) and (2.5) it follows that ratio F/P between the tangential and the normal force is constant and dependent on the properties of the bodies. We can identify this ratio with the friction coefficient, and so

$$\mu = \frac{s}{p}. \quad (2.6)$$

The relation (2.6) explains the independence of the friction force on the load and on the total area of contact. The fact that μ does not depend on the velocity is a consequence of the velocity independence of the bulk properties.

Among the possible critiques of the adhesion theory, one is particularly relevant. For elastic materials (like most hard rocks) the deformation at the asperities should be elastic. However, in the elastic limit, Hertz's theory predicts a nonlinear relationship between the area of contact and the load

$$A_r = kP^{2/3} \quad (2.7)$$

from which it follows that the friction coefficient should decrease with the load; moreover, the relationship between friction and load is nonlinear as well

$$\mu = skP^{-1/3}. \quad (2.8)$$

Whereas diamond does obey a relationship like (2.8), most rocks follow the linear behavior predicted by adhesion theory. The reason why an incorrect microscopic model of elastic compression predicts the correct macroscopic behavior is bewildering; it has probably to do with the geometrical arrangement of indenters. It has been shown that a model where many indenters of different sizes are distributed in hierarchies (a large indenter supports more smaller indenters of the same shape, each of which in turn supports the same number of smaller indenters, and so on) reproduces a linear friction in the limit of the number of hierarchies tending to infinite, although each indenter satisfies Hertz's law (Archard 1957; Scholz 2002).

2.1.2.4 Friction Coefficients for Rocks

Remarkably, friction coefficients for rocks turn out to depend little on the lithology. Data collected by Byerlee (1978) show that at overburden pressures lower than 200 MPa the average friction coefficient is

$$\mu \approx 0.85 \quad (\sigma < 200 \text{ MPa}). \quad (2.9)$$

This value should be considered as indicative. For example, some granites have friction coefficient between 0.6 and about twice as much, while some kinds of limestone have $0.70 < \mu < 0.75$. Other values of the friction coefficient are reported in the GeoApp. It is interesting to note that for higher pressures, $\sigma > 200$ MPa

$$\mu \approx \frac{50}{\sigma} + 0.6 \quad (\sigma > 200 \text{ MPa}) \quad (2.10)$$

showing that the friction coefficient slightly decreases with pressure, even though these values are beyond the pressure range of interest for landslides (200 MPa correspond to some 5–10 km of overburden rock).

Data reported in the tables and the fitting relations Eqs. 2.9 and 2.10 refer to polite surfaces. For asperities lengths less than some *mm*, the friction coefficient is independent of the roughness. However, interlocking between asperities greatly improves with surface roughness, with the effect of increasing the friction coefficient. In this case the effective friction coefficient is given by the Barton empirical formula (Barton 1973)

$$\mu_{\text{EFF}} = \tan \left[\tan^{-1}(\mu) + \text{JRC} \log_{10} \left(\frac{\sigma_j}{\sigma} \right) \right] \quad (2.11)$$

where σ_j is the compressive strength of rock (\rightarrow GeoApp) and JRC is called the roughness coefficient. Typical values for JRC range between 0 and 20 from very smooth to rough surfaces. In the field, the roughness can be measured by comparing the surface profile of rock with standard profiles. Roughness may be

very important for assessing rock stability in the presence of joints, but is of limited interest in dynamical studies of landslides, where rock is fragmented.

2.1.2.5 Final Form of the Friction Force to be Used in the Calculations

To summarize, the total horizontal force (gravity plus friction) acting on a body at rest on a plane inclined with angle β can be written as

$$\begin{aligned} F_{\parallel} &= 0 \\ &(\text{if } \tan \beta < \tan \phi \text{ and } U = 0) \\ F_{\parallel} &= Mg(\sin \beta - \cos \beta \tan \phi) \\ &(\text{if } U \neq 0 \text{ or } U = 0 \text{ and } \tan \beta \geq \tan \phi) \end{aligned} \quad (2.12)$$

2.1.2.6 Work Performed by Friction Forces

Let us consider again a block resting on a horizontal table. A force of magnitude greater than the static friction force, $Mg\mu = Mg \tan \phi$, is now applied to the body. Thrust by the external force, the block moves from an initial point A to a final position P during a certain time interval. The work performed by the friction force between A and P is

$$L(A \rightarrow P) = Mg \tan \phi \overline{AP} \quad (2.13)$$

where \overline{AP} is the curvilinear distance measured along the table (i.e., the trajectory length). For simplicity, we consider rectilinear trajectories. If the table is inclined with an angle β , a factor $\cos \beta$ has to be accounted for in the friction force, and the work becomes

$$L(A \rightarrow P) = Mg \tan \phi \cos \beta \overline{AP} = Mg \tan \phi R \quad (2.14)$$

where $R = \cos \beta \overline{AP}$ is the horizontal displacement. The last equation only follows if the displacement occurs along the slope direction.

If the inclination or the friction coefficient changes with the position, it is necessary to perform an integration

$$L(A \rightarrow P) = Mg \int_A^P \tan \phi \cos \beta dl \quad (2.15)$$

where dl is the line element along the trajectory. The integral returns again the total horizontal length, Eq. 2.14.

2.1.3 Cohesion

If a shear force is applied to a cube of muddy soil or rock at zero normal pressure, the resulting shear deformation is accompanied by a measurable resistance.

The resistance force per unit area is termed cohesion, and is measured in pascals (Pa). In natural soils, cohesion results from electrostatic bonds between clay and silt particles (\rightarrow Chap. 4). Thus, soils devoid of clay or silt are not cohesive except for capillary forces arising when little water forms bridges between sand grains, resulting in negative pore pressure (or “suction”). Values of soil cohesion typically are of the order of some kPa. In contrast, rocks normally exhibit much greater cohesion, thousands of times larger than soils.

At finite normal stresses, soils and rocks normally display both cohesive and frictional behavior. The shear strength of a soil is thus the sum of the cohesive and frictional contributions. Let us consider a slab of cohesive-frictional soil with constant thickness resting on a plane inclined with angle β . The resistive force is given by the combined effect of friction and cohesion in the following way

$$F_{\text{res}} = Mg \cos \beta \tan \phi + CwL \quad (2.16)$$

where w is the width of the slab and L is its length. If this combined force is lower than the gravity component along slope, the slab will not move. Because the mass is

$$M = \rho D w L \cos \beta \quad (2.17)$$

it is found that $F_{\text{res}} = \rho g D w L \cos^2 \beta \tan \phi + CwL$, or also

$$F_{\text{res}} = \sigma w L \tan \phi + CwL \quad (2.18)$$

where $\sigma = \rho g D \cos^2 \beta$ is the normal stress.

Finally, note that cohesion is also responsible for the finite value of tensile strength in both soils and rocks. The tensile strength, i.e., the tensile force per unit area, is normally a fraction of the cohesion.

An introduction to cohesion in soils is given by Selby (1993).

2.2 Slope Stability

2.2.1 A Few Words on Slope Stability

Gravity would tend to flatten out slopes, if it was not for the cohesion and friction forces of rocks and soils. However, the stability conditions may change due to temporary adjustments of equilibrium or because of external perturbations. In this case, a landslide may be triggered. There are numerous books and articles on slope stability. Here only a few basic examples are discussed to illustrate stability problems without any pretence of completeness.

The stability of a slope depends on several factors:

1. The kind of material involved. For example, recent volcanoclastic material may become very unstable and collapse into debris flows and lahars following



Fig. 2.3 A rock overhang unsupported at the base is an unstable condition that may lead to the detachment of portions of rock. Southern Norway

intense precipitation. In contrast, a hard and compact rock like intact gneiss is normally very stable.

2. The geometry of the material. Layers of rocks dipping toward slope are particularly unstable (Fig. 2.3). The slope angle is another important variable. The Frank landslide in Canada was probably due to instability along a bedding plane (Cruden and Krahn 1973).
3. The distribution of weight along slope. Loading the top of a slope may have great influence on stability. Likewise, cutting the slope at its base diminishes the buttressing of the lower layers underneath and promotes sliding conditions. This was particularly evident with the Betze-Post mine, where a mass of $3\text{--}10\text{Mm}^3$ of unconsolidated deposits showed a slow creep of some cm/day. Transferring some of the material from the top of the heap to the foot proved of immediate effect in diminishing the creep rate (Rose and Hungr 2007).
4. Water is one of the most important instability factors. It decreases cohesion in soils and increases weight and pore water pressure in granular media. The rate at which water seeps into the slope may also be critical. Some slopes may become unstable if even small amounts of water penetrate fast; others are more sensitive to the amount of water fallen in a long time span. The earthflow near Honolulu, Oahu, Hawaii, is a shallow (7–10 m) landslide that is periodically reactivated but only after massive precipitation. Recorded displacements do

not exceed some centimeters, however. More dramatic are the rapid flows that take place in many areas of the world where rock is blanketed by a thick layer of soil. Following intense rain, several landslides may be created at once, forming a characteristic barren landscape, like in the San Francisco area in 1982, or in the Sarno region in southern Italy in 1997 and 1998.

5. External impulsive forces such as earthquakes, waves, and volcanic eruptions. In July 1888, a swarm of strong earthquakes shook Mount Bandai, in Japan. A series of volcanic explosions, partly phreatic, destabilized a large portion of the summit, which collapsed in a debris avalanche covering an area of 3.5 km^2 . Better known is the eruption of the St. Helens of March 1980. A flank of the volcanic edifice slowly bulged during the 1980 activity following more than a century of dormancy. The progressive deformation finally resulted in a giant collapse and a debris avalanche with approximate run-out of 30 km. Following the landslide, the pressure underneath the northern sector of the edifice plummeted, which caused the strong blast recorded in the photographs.
6. Vegetation may influence stability through mechanical cohesion and removal of water via evapotranspiration.

2.2.1.1 Factor of Safety

To quantitatively assess the stability of a slope in engineering geology, a parameter F known as *factor of safety* is introduced. The factor of safety is the ratio between the resistive forces and gravity pull

$$\text{Factor of safety } F = \frac{\text{Resistance forces}}{\text{Gravity force parallel to slope}} \quad (2.19)$$

A value $F > 1$ indicates stability, whereas $F < 1$ implies instability. Thus, the transition between stability to collapse may be envisaged mathematically as a decrease in the factor of safety to values below unity.

2.2.2 An Example: Layered Slope

A simple model of stability analysis consists in analyzing a homogeneous slope like in Fig. 2.4, including the possible presence of water at a certain depth. From Eq. 2.18, the resistive forces deriving from cohesion and friction can be written in the following way

$$F_{\text{res}} = CwL + (\sigma - P_w)wL \tan \phi. \quad (2.20)$$

where the effect of water resulting in pore pressure P_w has been added. Water tends to destabilize the slope, because as evident from Eq. 2.20, it acts in the direction

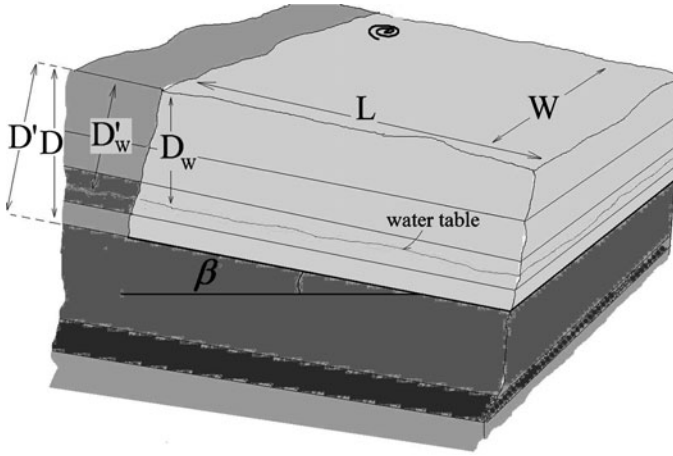


Fig. 2.4 Layered slope for the calculation of the factor of safety F

of reducing the contribution of the effective friction angle. The water table is assumed to lie at a constant depth. Because the normal pressure is (\leftarrow Sect. 2.1)

$$\begin{aligned}\sigma &= \rho g D \cos^2 \beta \\ P_w &= \rho_w g (D - D_w) \cos^2 \beta\end{aligned}\quad (2.21)$$

it is found that

$$F_{\text{res}} = C_w L + (\Delta \rho D + \rho_w D_w) g w L \cos^2 \beta \tan \phi \quad (2.22)$$

whereas accounting also for the weight of pore water

$$F_p = [\rho D + \rho_w \chi (D - D_w)] g w L \sin \beta \cos \beta \quad (2.23)$$

where $\chi < 1$ is the volume fraction of water for the case of 100% saturation. Considering that $\rho D \gg \rho_w \chi (D - D_w)$, this term can be neglected for simple estimates.

The factor of safety becomes so

$$\begin{aligned}F &= \frac{F_{\text{res}}}{F_{\text{=}}} = \frac{\tan \phi}{\tan \beta} \left(\frac{\Delta \rho}{\rho} + \frac{\rho_w D_w}{\rho D} \right) + \frac{C}{D \rho g \sin \beta \cos \beta} \quad \text{if } D_w < D \\ F &= \frac{F_{\text{res}}}{F_{\text{=}}} = \frac{\tan \phi}{\tan \beta} + \frac{C}{D \rho g \sin \beta \cos \beta} \quad \text{if } D_w \geq D\end{aligned}\quad (2.24)$$

If a tensile stress C_T contributes to stability along the surface of area WD , then (2.24) can be generalized to

$$F = \frac{F_{res}}{F_{=}} = \frac{\tan \phi}{\tan \beta} \left(\frac{\Delta \rho}{\rho} + \frac{\rho_w D_w}{\rho D} \right) + \frac{1}{\rho g \sin \beta \cos \beta} \left[\frac{C}{D} + \frac{C_T}{L} \right] \quad \text{if } D_w < D$$

$$F = \frac{F_{res}}{F_{=}} = \frac{\tan \phi}{\tan \beta} + \frac{1}{\rho g \sin \beta \cos \beta} \left[\frac{C}{D} + \frac{C_T}{L} \right] \quad \text{if } D_w \geq D$$
(2.25)

As a simple application, let us assume absence of water. Imposing $F > 1$ we find the condition of instability as

$$\tan \beta > \frac{1}{\rho g \cos^2 \beta} \left[\frac{C}{D} + \frac{C_T}{L} \right] + \tan \phi. \quad (2.26)$$

The cohesive term (first term on the right-hand side) becomes very small for long and deep slabs, $\rho g D \gg C$ and $\rho g L \gg C_T$; thus, cohesion in soils is particularly important for a shallow landslide. In compact rocks, where cohesion and tensile stress typically reach values of tens of MPa, the cohesive term may become important also for large landslides.

It is also interesting to solve for D as a function of the angles

$$D > \frac{1}{\tan \beta - \tan \phi} \frac{C}{\rho g \cos^2 \beta}. \quad (2.27)$$

where the contribution from the tensile strength has been neglected for simplicity. This equation shows that a minimum thickness is necessary for instability to occur. If the angle of dipping approaches the friction angle, the minimum thickness tends to infinity. Thus, landslides developing at angles close to the friction angle will be particularly large (Cruden and Krahn 1973).

If cohesion is more important than friction in stabilizing the slope, assuming $L \gg D$ one obtains the depth of detachment as

$$D = \frac{C}{\rho g \sin \beta \cos \beta}. \quad (2.28)$$

It is sometimes observed that the pressure of water is greater than that of the hydrostatic value. This may occur, in particular, when the soil permeability is low so that pressurized water cannot seep to zones of lower pressure. By inserting a pipe in the soil at the height of the water level, water will rise up in the pipe to a height η , called the piezometric height. Formally, another pressure term should be added to Eq. 2.21 accounting for the excess pressure. In practice, however, it is better to directly write the equations in terms of the piezometric height η previously measured on the terrain

$$P_w = \rho_w g \eta \quad (2.29)$$

and so the factor of safety becomes

$$F = \frac{\tan \phi}{\tan \beta} \left(1 - \frac{\rho_w \eta}{\rho D} \right) + \frac{1}{\rho g \sin \beta \cos \beta} \left[\frac{C}{D} + \frac{C_T}{L} \right] \quad (2.30)$$

Box 2.1 One Step Back: The Stress Tensor

The present Box is rather concise. A more thorough presentation can be found in Middleton and Wilcock (1994).

Some physical properties, like the temperature of a body, can be described by just one number. These quantities are called *scalars*. Other quantities, *vectors*, require three numbers. The velocity of a material point is an example of vector quantity. The existence of three components derives from the three-dimensionality of space. In Cartesian coordinates, the vector components are the projections of the vector along the directions in space x , y , and z . Vectors satisfy certain transformation rules between different reference systems. This is because a vector has an essence in itself, which is independent of the reference system used to represent it. Mathematically, this has the consequence that, although the components of a vector depend on the reference system, its components are linked to the specific condition that the vector magnitude (i.e., its length) should be the same in all reference systems.

Other physical quantities necessitate an extension of the concept of vector. The state of stress of an elastic body is described by a *tensor*, a mathematical object of nine components. Let us consider an infinitesimal cube like in Fig. 2.5. Let the six faces be perpendicular to the directions of the Cartesian coordinates. We label with the letter “ x ” the two faces perpendicular to the coordinate x , and similarly we do with the other faces. Of the six faces, in Fig. 2.5, we consider only the three facing the observer. These faces are denoted as “positive” because the directions x , y , and z of the coordinate

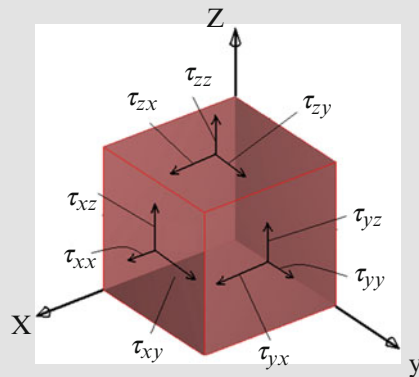


Fig. 2.5 For the definition of the stress components

(continued)

Box 2.1 (continued)

system cross the cube faces from the interior outwards. In other words, a positive face is a face whose outer normal points in the positive direction. On the surface of the positive “ x ” face we can draw a vector with its three Cartesian components along x , y , and z . We call these components τ_{xx} , τ_{xy} , τ_{xz} , respectively. In this notation, the first index identifies the face; the second index denotes the direction of the vector component. Thus, τ_{xy} is the component y of the vector acting on the face x of the figure. Similarly, we introduce the other components τ_{yy} , τ_{yx} , τ_{yz} , τ_{zz} , τ_{zx} , τ_{zy} . We call tensor the mathematical object so defined.

So far, the definition of tensor has been purely formal, as no particular significance was attributed to the vectors of the form τ_{xy} . We now specify the equations to an important mathematical object used in continuum mechanics, the stress tensor. Suppose that the elementary cube shown in Fig. 2.5 resides within a larger volume of material subjected to an external stress, for example a portion of rock on which tectonic lateral thrust in addition to gravity is acting. The external stress field will act on the three faces of the elementary cube through three stress vectors on each of the front faces of the cube. In turn, each of these stress vectors can be decomposed into three components, for a total of nine vectors. For example, the stress vector acting on the x face is evidently

$$\vec{\tau}_x = \tau_{xx}\hat{i} + \tau_{xy}\hat{j} + \tau_{xz}\hat{k} \quad (2.31)$$

where $\hat{i}, \hat{j}, \hat{k}$ are the versors (i.e., vectors of unit magnitude) pointing in the directions x , y , and z , respectively. Similar equations specify the stress vector on the other two frontal faces of Fig. 2.5. One might question why the other three faces of the cube (the negative ones) are not considered. This is because according to the standard geometrical construction of Fig. 2.5, the other three back faces belong to the front faces of another neighboring cube.

We can thus specify these nine numbers as the component of stress in a medium. This particular Cartesian tensor is denoted as the stress tensor, and provides the state of stress within the entire volume of the medium. The components τ_{xx} , τ_{yy} , τ_{zz} are called diagonal; the components τ_{ij} with $i \neq j$ are denoted as the off-diagonal terms. The denomination derives from the possibility to represent the component of the stress tensor in a matrix, i.e., a square table of the form

$$\begin{pmatrix} \tau_{xx} & \tau_{xy} & \tau_{xz} \\ \tau_{yx} & \tau_{yy} & \tau_{yz} \\ \tau_{zx} & \tau_{zy} & \tau_{zz} \end{pmatrix}. \quad (2.32)$$

(continued)

Box 2.1 (continued)

A component of stress is positive when it is directed toward the positive axis of the reference system, and on a positive face. The components shown in Fig. 2.5 are positive. Likewise, the stress is positive if it points in the negative direction of a negative face. A component is negative if it points in the negative direction of a positive face, or in the positive direction of a negative face. As an example of negative component, think changing direction to the component τ_{xx} in Fig. 2.5. The opposite definition can also be found (and is adopted in the calculation of \rightarrow Sect. 2.2.3 for convenience), where a positive component of the stress tensor is associated to the positive direction of a negative face.

An important property of the stress tensor is its symmetry, i.e., the equality between off-diagonal components with exchanged indices, namely: $\tau_{xy} = \tau_{yx}$; $\tau_{xz} = \tau_{zx}$; $\tau_{yz} = \tau_{zy}$. This condition results from stability considerations on the elementary volume. If for example were $\tau_{xy} \neq \tau_{yx}$, the torque directed along z acting on the elementary volume would be unbalanced, and the equations of dynamics would predict it to spin around the z axis. For very small volumes (the cube is infinitesimal) the spinning rate would tend to an infinite value. These symmetry conditions reduce the independent components of the stress tensor from nine to six. In two-dimensional problems, the independent stress tensor components are evidently three.

The diagonal components of the stress tensor are called the normal stresses, and are often denoted with the Greek symbol sigma: $\sigma_x, \sigma_y, \sigma_z$. The nondiagonal components of the stress tensor are called shear stresses. It is always possible to find a local reference system such that the shear stresses $\tau_{xy}, \tau_{xz}, \tau_{yz}$ vanish, and the state of stress is specified by the sole diagonal components. This procedure, also called diagonalization, is schematized in Fig. 2.6. The three diagonal stress vectors so identified ($\bar{\tau}_{xx}, \bar{\tau}_{yy}, \bar{\tau}_{zz}$ or also $\bar{\sigma}_x, \bar{\sigma}_y, \bar{\sigma}_z$) are called the principal stresses. In other words, diagonalization corresponds in finding the three perpendicular planes for which the shear stresses are zero. The recipe to find the principal stresses is sketched in the MathApp.

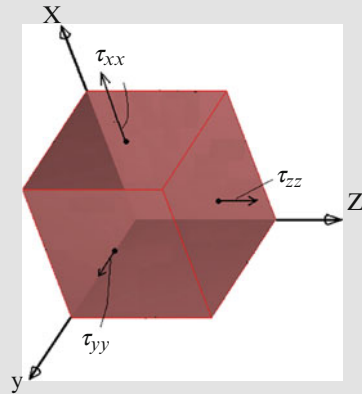
A final set of definitions will be useful for the following discussions. Once we have identified the magnitude and the direction of the principal stresses throughout each point of a stressed elastic body, it is possible to draw three families of lines parallel to the three principal stresses (only two will be necessary in two dimensions). These lines are called the stress trajectories, and give a clear-cut picture of the state of stress in the body.

How will a particular material respond to a certain stress field? It is obvious that a stiff material will deform less than a soft one for the same stress. Thus, to answer this question, further equations specifying the material properties are needed. In particular, two kinds of materials are relevant

(continued)

Box 2.1 (continued)

Fig. 2.6 Geometrical interpretation of the tensor diagonalization. At a certain point, a particular orientation of the local reference system reduces the tensor in a diagonal form



for the following discussion, which give different relationships between the stress and the deformation:

1. Some materials, such as the elastic ones, exhibit a relationship between the stress and the deformation. The state of stress in an elastic medium is specified in terms of the Navier equation, which is beyond the scope of the book (see, e.g., Middleton and Wilcock 1994).
2. For a different class of materials, the relevant relationship is between the stress and the deformation rate. These are the plastic and liquid substances. The resulting relations are the basis of fluid mechanics and will be explored in detail in Chaps. 3 and 4.

Box 2.2 Example of Stress Tensors in Stability Problem

Let us consider the case of an infinite outcrop of rock. Choosing the z direction parallel to the vertical, we seek for the expression of the stress tensor at a depth D under the surface. The zz component is evidently given as $\tau_{zz} = \rho g D$. This is the stress that would be measured by a pressure transducer oriented with the vertical face. The other two diagonal components xx and yy depend on the type of material. Elastic materials like hard intact rock follow the Hooke behavior (\rightarrow Sect. 5.1.1) for which $\tau_{xx} = \tau_{yy} = \frac{\nu}{1-\nu} \tau_{zz} = \frac{\nu}{1-\nu} \rho g D$. With the Poisson coefficient ν typically of the order 0.25, the xx and yy components are about 30% smaller than the component zz . The stress tensor becomes so

(continued)

Box 2.2 (continued)

$$\begin{pmatrix} \frac{\nu}{1-\nu}\rho g D + \Sigma & 0 & 0 \\ 0 & \frac{\nu}{1-\nu}\rho g D & 0 \\ 0 & 0 & \rho g D \end{pmatrix} \quad (2.33)$$

where the shear terms vanish due to the symmetry. Further notice that independent stresses sum up linearly. Thus, if a constant tectonic stress of magnitude Σ is acting horizontally along the xx component, its contribution appears summed to the corresponding matrix term, as shown in (2.33).

A graphic way of illustrating the stress field within a stressed medium is by using the stress trajectories, (i.e., lines parallel at each point to the directions of the principal stresses, ←Box 2.1). Stress trajectories for the previous problem are drawn in Fig. 2.7 (exploiting the invariance along the horizontal direction, we can draw the stress trajectories in just two dimensions). In this particular case, they are simply a network of two families of straight lines, respectively, parallel and perpendicular to the ground. Another useful concept is the one of stress ellipsoid. At each point of the stressed medium, an ellipsoid can be drawn with axes equal to the magnitude of the three principal stresses and oriented as the principal stresses. In two dimensions, the ellipsoid becomes an ellipse. The stress ellipse is shown in Fig. 2.7 for the example above.

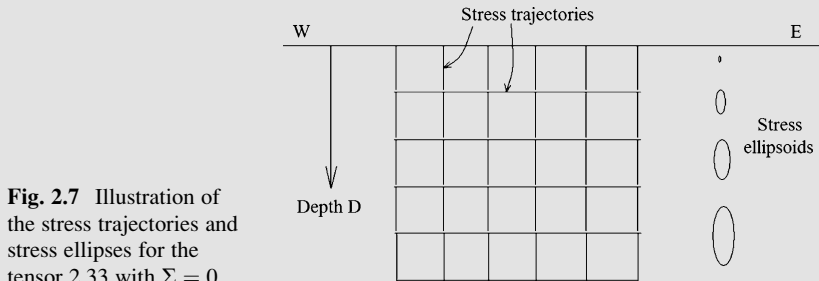


Fig. 2.7 Illustration of the stress trajectories and stress ellipsoids for the tensor 2.33 with $\Sigma = 0$

2.2.3 A Few Basics Concepts of Soil Mechanics and an Application to Slumps

In contrast to a layered slide like that of Fig. 2.4, in homogeneous soils there are no leading weakness layers. The surface of rupture thus develops following the internal and external forces, rather than on the preexisting geometry. The most likely surface of detachment is the one that gives the smallest factor of safety. The detachment surface that minimizes the factor of safety turns out to be sub-spherical, or spoon-like shaped. The corresponding landslide is thus a rotational

slide or *slump*. To understand the mechanical origin of the spoon-like shape of this kind of landslides, let us briefly introduce first some elementary concepts of soil mechanics, which will also be useful in other contexts.

2.2.3.1 Mohr Circle

Consider a two-dimensional prism like in Fig. 2.8, making an angle β with respect to the horizontal. Both shear and normal stresses act on the prism from the lower “B” and left “A” faces of the figure. We wish to calculate the shear and normal stresses τ and σ acting on the upper tilted face denoted as “S.” Consider the force

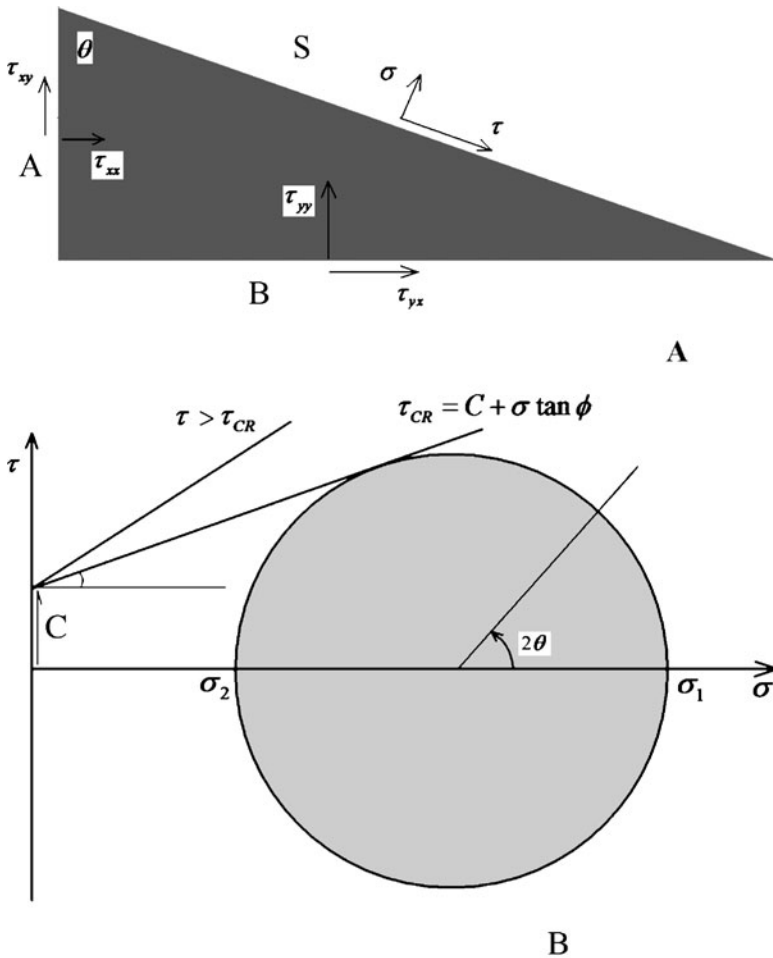


Fig. 2.8 Upper: equilibrium of a small prism. Lower: the Mohr circle of stress

on S directed to x , that we call S_x . The forces contributing to S_x are two shear forces and two normal forces acting on the faces A and B , for a total of four. Because the prism is in equilibrium, $S_x = 0$. Similarly, the four forces directed vertically on the faces A and B sum up to give the total force S_y acting on S and directed along y . To obtain the normal and shear stresses on S , the resultant forces S_x and S_y are projected along the directions normal and parallel to S . Dividing by the areas of the faces finally provides the stresses. The result for the stress on S , respectively, normal and shear reads

$$\begin{aligned}\sigma &= \frac{1}{2} \tau_{xx} [1 + \cos(2\theta)] + \tau_{xy} \sin(2\theta) + \frac{1}{2} \tau_{yy} [1 - \cos(2\theta)] \\ \tau &= \frac{1}{2} (\tau_{xx} - \tau_{yy}) \sin(2\theta) - \tau_{xy} \cos(2\theta).\end{aligned}\tag{2.34}$$

Evidently, for $\theta = \pi/2$ the face S becomes horizontal and $\sigma = \tau_{yy}$; $\tau = \tau_{xy}$. For $\theta = \pi/4$ (S at 45° with respect to the horizontal) it follows $\sigma = \frac{1}{2} (\tau_{xx} + \tau_{yy}) + \tau_{xy}$; $\tau = \frac{1}{2} (\tau_{xx} - \tau_{yy})$. For $\theta = 0$ (surface “P” vertical) $\sigma = \tau_{xx}$; $\tau = -\tau_{xy}$.

Consider now a situation where the stress tensor is in diagonal form so that there are no shear stresses acting on the A and B surfaces. Evidently, in this case the equations for σ and τ are similar to (2.39), but with the following replacements: $\tau_{xx} = \sigma_1$; $\tau_{yy} = \sigma_2$; $\tau_{xy} = 0$ where σ_1 , σ_2 are the two principal stresses. Equation 2.34 becomes so

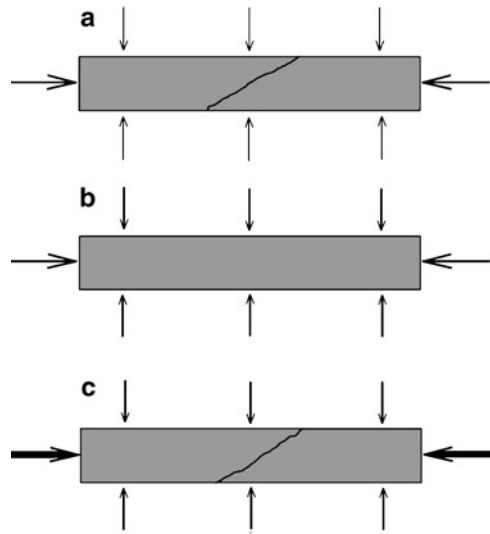
$$\begin{aligned}\sigma &= \frac{1}{2} \sigma_1 [1 + \cos(2\theta)] + \frac{1}{2} \sigma_2 [1 - \cos(2\theta)] \\ \tau &= \frac{1}{2} (\sigma_1 - \sigma_2) \sin(2\theta)\end{aligned}\tag{2.35}$$

The first equation of (2.40) can also be rewritten as

$$\sigma = \frac{1}{2} (\sigma_1 + \sigma_2) + \frac{1}{2} (\sigma_1 - \sigma_2) \cos(2\theta)\tag{2.36}$$

and the shear stress τ can now be plotted as a function of σ with the angle θ varying parametrically. The locus is a circle of center $\frac{1}{2}(\sigma_1 + \sigma_2)$ and radius $\frac{1}{2}(\sigma_1 - \sigma_2)$, called the Mohr circle (Fig. 2.8b). The circle gives a pictorial view of the behavior of the normal and shear stresses with changing inclination angle of a plane with respect to the direction where the stress tensor is diagonal. For $\theta = 90^\circ$ ($\sigma = \sigma_1$; $\tau = 0$) the S plane is horizontal. Likewise, when $\theta = 0^\circ$ the S plane is vertical and the shear stress vanishes. For a generic value of θ the surface S is inclined and both the normal and shear stresses acquire a nonzero value. The maximum shear stress, reached on top of the circle, is found for $\theta = \pi/4 = 45^\circ$.

Fig. 2.9 (a) If a sample of frictional-cohesive rock or soil is subjected to constant confining pressure (vertical arrows) and compressive stress (horizontal arrows), it typically fails at an angle greater than 45° . If the confining pressure is increased (b), a point is reached where the material will not fail for the same compressive stress. The compressive stress must be increased for failure to occur (c)



2.2.3.2 Failure Criterion for a Cohesive-Frictional Material

Mohr's circle allows also a graphic representation of the failure of cohesive-frictional soil or rock. Experiments show that cohesive-frictional materials fracture at angles θ slightly greater than 45° (Fig. 2.9).

The Navier–Coulomb criterion states that fracture occurs when the shear stress exceeds a critical value given as

$$\tau_{CR} = C + \sigma \tan \phi \quad (2.37)$$

where ϕ is the internal friction angle and C is the cohesion. Note that the normal pressure has a stabilizing effect, raising the critical shear stress required for failure. The geometrical locus of τ_{CR} as a function of σ is a straight line, which is also reported in Fig. 2.8b. If the line does not intersect the Mohr circle, the shear stress in the medium is not exceeded and the material does not break. The line tangent to the Mohr circle corresponds to the critical situation when rupture is about to occur. From the geometry of the figure, the critical angle for failure becomes

$$\theta_{CR} = \frac{\pi}{4} + \frac{\phi}{2} = 45^\circ + \frac{\phi}{2}. \quad (2.38)$$

2.2.3.3 Slumps

Consider now a slope with a step like in Fig. 2.10. The two families of stress trajectories for this particular case are shown in Fig. 2.10a, b. Because the two

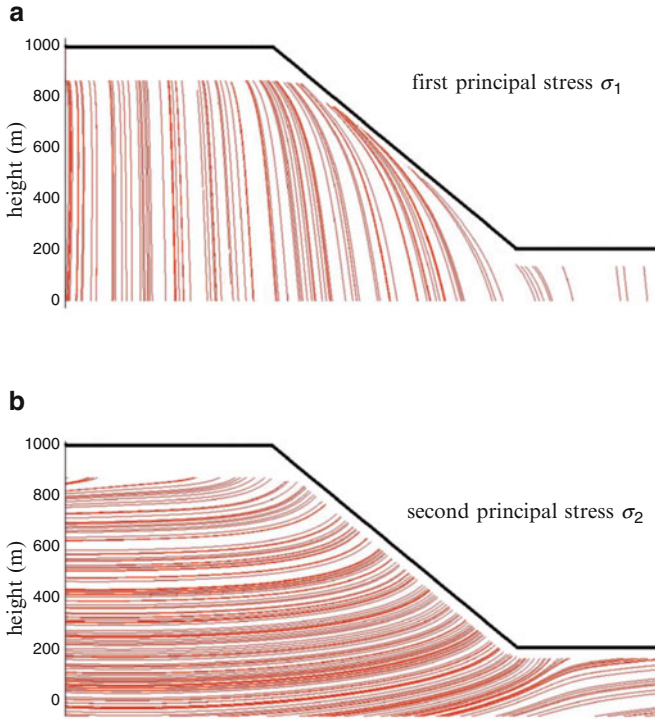


Fig. 2.10 Stress trajectories in an elastic medium with the properties of granite

principal stresses are mutually perpendicular at every point, the two families of stress trajectories are perpendicular too (this problem is two-dimensional so there is no third principal stress). Consider now the point of intersection of two stress trajectories as shown in Fig. 2.11. The failure is more likely to occur along a line inclined by $45^\circ \pm \phi/2$ with respect to the directions of the two principal stresses. One of these lines is schematically shown in Fig. 2.11; it does assume a sub-circular form, so outlining the concave form of slumps.

Let us fix one point deep in the soil, for example one of the coordinates $x = 1,500$ m; $y = 200$ (the orientation of the global reference system is chosen with the x and y axes parallel and perpendicular to the base, respectively). The shear and the normal stresses are measured along the planes A , B , and C of Fig. 2.11. Because the step is just a small perturbation at such depth, a resulting small value for the shear stress will be measured in A . The plane A is nearly parallel to the principal stress τ_{xx} ; thus, the normal stress recorded in A is close to τ_{yy} . The plane B of Fig. 2.11 measures the component τ_{xx} of the stress tensor. It has been shown (\leftarrow Box 2.2) that in elastic media the stress component τ_{xx} is proportional to τ_{yy} . In frictional soils a relationship of proportionality

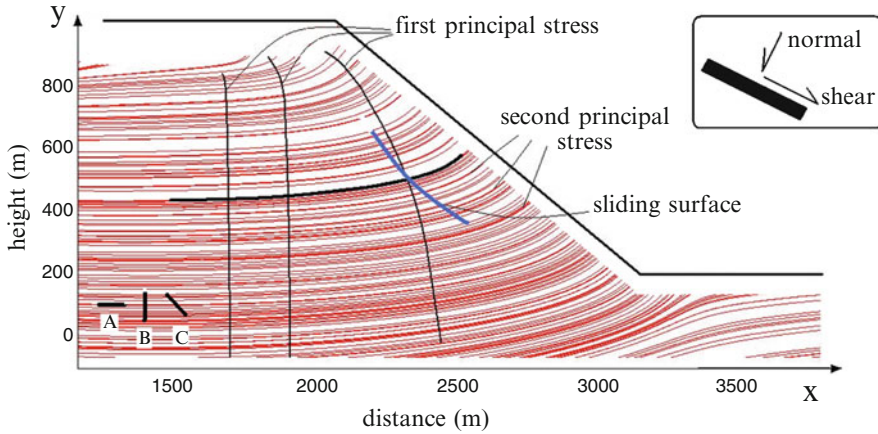


Fig. 2.11 The surface of detachment of a slump

$$\tau_{xx} = k\tau_{yy} \quad (2.39)$$

also holds where k , called the coefficient of earth pressure, depends on the state of tensional-compression state of the medium. If the medium is compressed (corresponding to the so-called Rankine passive state) the coefficient is greater than unity. If the medium is expanding laterally (Rankine active state), the coefficient is lower than unity. If the medium is static there is an indeterminacy as to the actual value of the earth pressure coefficient, which falls somewhere between the active and the passive values. At failure, the Mohr circle is tangent to the line $\tau_{CR} = C + \sigma \tan \phi$. Thus, the radius of the circle is fixed, and so the ratio σ_2/σ_1 can be determined. This ratio corresponds to the earth pressure coefficient at failure. The situation in which the lateral stress is smaller than the vertical stress corresponds evidently to the active case, and is the one of more interest for landslides, because failure normally occurs during a tensional phase. The result is

$$\tau_{xx} = \frac{1 - \sin \phi}{1 + \sin \phi} \tau_{yy} + 2C \frac{\cos \phi}{1 + \sin \phi}. \quad (2.40)$$

Notice also that τ_{xx} may become negative for very small τ_{yy} . Remembering that $\tau_{yy} = \rho g D$ where D is the depth, this implies that the lateral stress close to the surface is negative for cohesive soil. The result is the formation of tension cracks in regions of soil instability that heal at sufficient depth (see also the opening figure of the chapter). Coming back to Fig. 2.11, note that the stress in the point C has a shear component in addition to the normal component.

Figure 2.13 shows a small slump in cohesive soil (top) and cracks in the soil of an unstable area (bottom).

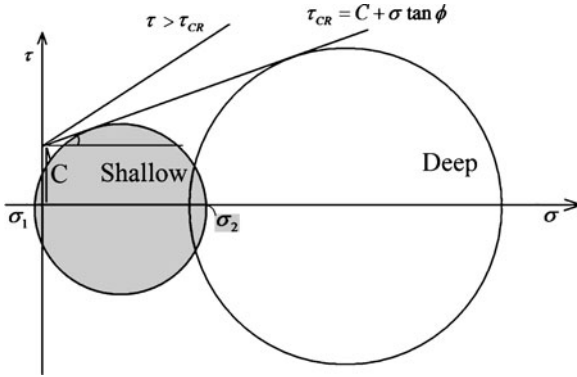


Fig. 2.12 The Mohr circle for a deep soil layer at failure is shown with the large circle. In a shallower layer at failure conditions, the circle shifts to the *left*, always remaining tangent to the Mohr–Coulomb line. A point is reached where the smaller of the principal stresses becomes negative (*small, gray circle*). This shows the existence of a state of tension at the surface. The finite value of cohesion C is necessary for the existence of a tensional state

2.2.3.4 Factor of Safety and a Simple Criterion for a Rotational Slide

In a first approximation, the shape of a rotational slide can be assumed as part of a circle of length L (Fig. 2.14). Because the driving force is the gravity acting on the center of mass which is displaced horizontally from the center of the circle, a torque develops of magnitude equal to

$$m = MgX - CLRW \quad (2.41)$$

where W is the width (perpendicular to the drawing), M is the mass, and X is the horizontal distance between the center of mass and the center of the circle. We have also assumed a purely cohesive material, absence of friction, and invariance along the direction perpendicular to the figure. Imposing that the torque > 0 , the condition of instability becomes

$$X \geq \frac{CLR}{(M/W)g} \quad (2.42)$$

while the factor of safety is defined as the ratio between the moment of the resistance forces and the torque (Fig. 2.14).

$$F = \frac{CLR}{(M/W)gX} \quad (2.43)$$

Note that because the geometrical quantities scale as

$$L \propto R; \quad M/W \propto R^2; \quad X \propto R, \quad (2.44)$$

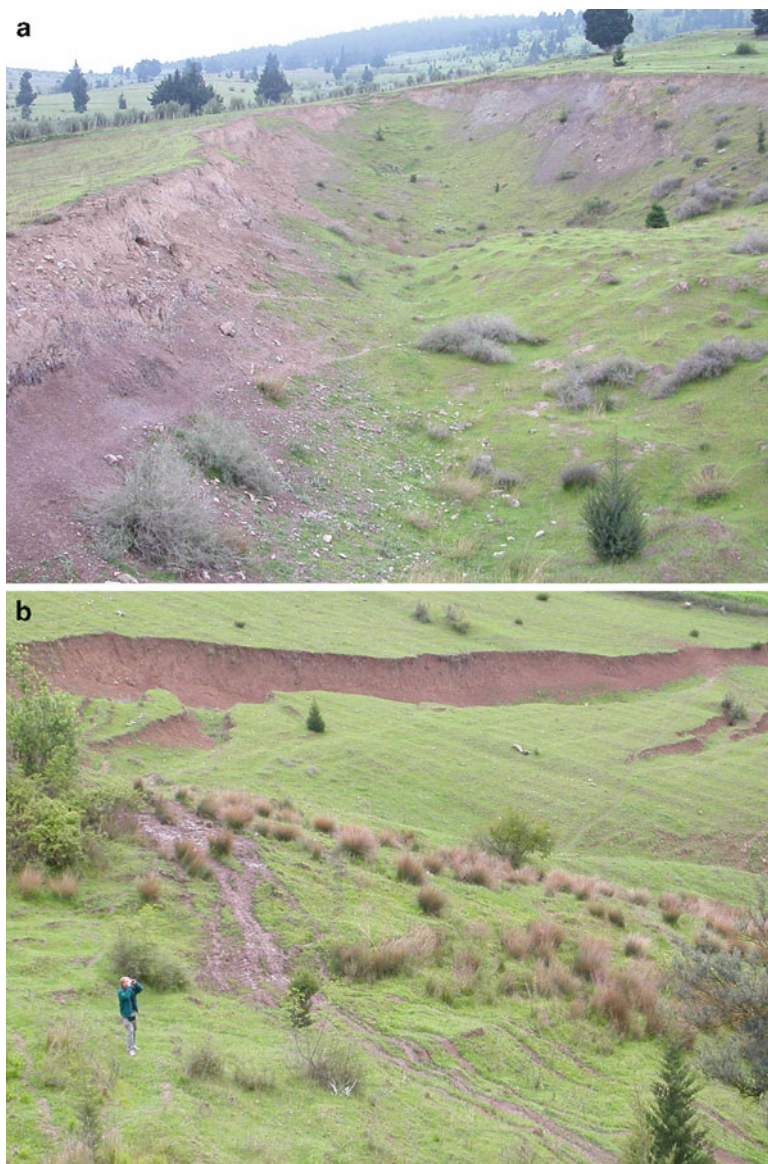


Fig. 2.13 (a) A small slump in soft terrain. (b) A new slump is often preceded by tension cracks. Both near Fatalak, northern Iran. See also the figure at the beginning of the chapter. Impulsive forces may result from earthquakes. Water seeping into the terrain may have diminished cohesion and friction and promoted instability, but the final trigger of this landslide was an earthquake on a previously unstable terrain

Fig. 2.14 The torque acting on a rotational slide

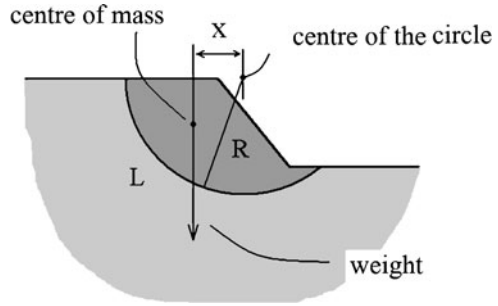
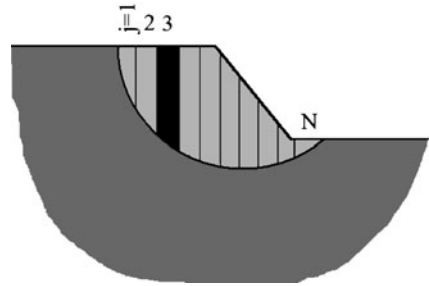


Fig. 2.15 According to the Fellenius method, the slump is divided into vertical slices and the factor of safety is obtained summing up the contribution of each slice to both gravity and resistance



it follows that $F \propto 1/R$, i.e., the factor of safety decreases with the radius of the slump. For this reason, the rotational slides require a minimum radius to develop.

For a soil with nonzero friction angle, the calculation is more complicated because the resistance is proportional to the local thickness of the slump. Several methods have been developed to calculate the factor of safety in this case. The rupture surface is initially conjectured. The landslide material is divided into segments separated by parallel, vertical sectors like in Fig. 2.15. Each sector, identified with a progressive number “ j ,” contributes to a shear resistance in the form

$$(P_j \cos \beta_j - u \delta L_j) \tan \phi + C \delta L_j \quad (2.45)$$

where P_j is the weight of each sector and δL_j is the arc length. The shear stress is evidently $P_j \sin \beta_j$, so that the factor of safety can be obtained summing up all the contributions from each sector

$$F = \frac{\sum_{j=1}^N (P_j \cos \beta_j - u \delta L_j) \tan \phi + CL}{\sum_{j=1}^N P_j \cos \beta_j} \quad (2.46)$$

The weight P_j can be calculated from the geometry of the slice and the density of the material. Note that also soils with nonuniform properties may be considered in

the calculations. This method, called the ordinary method of slices (or also the Fellenius method) is often used in analytical estimates of stability, although a computer will speed-up the calculations for complicate shapes and allow for numerous slices. It has some drawbacks, however. It does not consider properly the curvature of the sliding surface, and the Earth pressure force is not accounted for. This is reflected in characteristically low values of the factor of safety (of the order 10–15%) compared to those obtained with more advanced models. For this reason, methods like the modified Bishop method are currently used. In this method, the calculation of the factor of safety F is more involved, as it requires previous knowledge of F itself. With the use of modern computers, however, an iterative convergence of the solution can be easily attained. These methods are described at some length by Duncan (1996).

2.2.4 Other Factors Contributing to Instability

Numerous landslides are caused by earthquakes. The first documented suggestion is due to Dante Alighieri in the thirteenth century who mentions in the *Divine Comedy* the “tremuoto” (i.e., earthquake) as possible trigger for the Lavini di Marco landslide in Northern Italy (→Chap. 6). However, it is only with the seismic swarm of 1783 in Calabria (southern Italy) that the correlation between earthquakes and landslides began to be studied scientifically (Keefer 2002). All kinds of slides can be potentially triggered by earthquakes: approximate magnitudes necessary to produce a failure range from a modest $M = 4$ for rock falls to $M = 6$, $M = 6.5$ for rock and soil avalanches (Keefer 2002). Many devastating landslides have been triggered by earthquakes, such as the Nevados Huascaran rock and ice avalanche (→Chap. 6).

Correlations have been suggested between the area affected by landslides and the magnitude of the quake. For example, based on data fit a relationship of the form has been suggested (Keefer 2002)

$$\log_{10} A(\text{km}^2) = M - 3.46(\pm 0.47) \quad (2.47)$$

An earthquake of magnitude $M = 7$ can so potentially affect an area of about 10,000 km².

Physically, the action of earthquakes is to temporarily increase the ratio $\frac{\Delta\tau}{\sigma}$ between earthquake-induced shear stress and normal pressure.

In addition to increasing the shear stress, earthquakes may also liquefy water-saturated sands. During the shock, grains partially rest on the fluid rather than on other grains. When the contact between grains is lost, the pore water pressure tends to become equal to the total pressure. Hence, the soil is transformed into a dense liquid mixture of water and sand. This was the condition to blame when the Kensu debris flow (China) killed 200,000 people in 1920. During liquefaction, the ratio $\frac{\Delta\tau}{\sigma}$ can be estimated with the Seed–Idriss formula valid for depths $D < 12$ m

$$r = \frac{\Delta\tau}{\sigma} = 0.65(1 - 0.008D) \frac{a_{\max}}{g} \frac{P_N}{P_N - P_A} \quad (2.48)$$

where a_{\max} is the maximum soil acceleration, P_N , P_A are the normal pressure without the effect of the quake, and the water pressure, respectively. Earthquakes of magnitudes 5, 6, 7, and 8 generate accelerations of 0.06, 0.15, 0.5, and 0.6 g, respectively, in the epicenter region. Thus, the ratio $\frac{\Delta\tau}{\sigma}$ may grow up to 0.5 for strong earthquakes. Far from the epicenter, the acceleration of the terrain during a quake decreases markedly. For example, at a distance of 10–100 km the acceleration is reduced by 53% and 13% of the epicenter value, respectively.

Vegetation may alter the stability of superficial soils, too. Firstly, roots may help stabilize the slope partly because they deprive the soil of water, and also as a consequence of their mechanical action similar to natural reinforcement shafts. However, vegetation may also have a negative impact on stability. Some species of bushes may increase instability by promoting the catchment of superficial water. In addition, trees add weight to the slope, an effect that may be significant for superficial soils. To deal with stability change, a factor ΔC is formally added in the equation for the factor of safety so that

$$F = \frac{\tan \phi}{\tan \beta} + \frac{1}{\rho g \cos \beta \sin \beta} \left[\frac{C + \Delta C}{D} + \frac{C_T}{L} \right] \quad (2.49)$$

Values for ΔC have been collected for example by Sidle and Ochiai (2006). Maximum values may reach $\Delta C \approx 20$ kPa, but lower figures in the range of some kPa are more typical.

Box 2.3 External Link: Are Glacial Cirques the Remains of Ancient Landslide Scars?

Glacial cirques are typical mountain landforms well-known to both geomorphologists and mountaineers. They have the shape of an upside-down helmet with steep wall, and typical width between 400 and 800 m. Cirques often punctuate the mountain environment at altitudes higher than the firn line (i.e., the level where the snow retreats during the thaw season). Cirques at lower altitude in the Alps are ascribed to a lower firn line corresponding to the coldest climate during the glaciations. Cirque size is not much dependent on the past history and glacial characteristics of the area. In a way, cirques represent a deviation from the fractal-like character of mountain altitudes, which is otherwise characterized by a power-law distribution of the topography spectral density.

The standard model of cirque development considers equally important the periglacial and glacial processes. Periglacial processes commence when snow drifts into a hollow, a process termed nivation; freeze-thaw cycles are

(continued)

Box 2.3 (continued)

then responsible for headwall retreat until the hollow reaches a critical size. As the snow gathers in sufficient amount to form a small cirque glacier, the process of cirque excavation and wall retreat continues due to direct ice abrasion.

An alternative hypothesis for the formation of glacial cirques has been recently suggested (Turnbull and Davies 2006). The authors consider the measured erosion rates of glacial cirques as too low to explain the depth of most cirques (500 m in some cases). If cirques mostly grow due to glacier erosion, then it is reasonable as a working approximation to assume an erosion rate proportional to the shear stress at the base of the cirque glacier, and so

$$\frac{dy}{dt} = ky. \quad (2.50)$$

which for a constant value of k gives an exponential increase. This parameter is estimated from erosion measurement as $\approx 3 \times 10^6 a^{-1}$. Thus, it takes over one million years to excavate the cirque, which is more than the duration of the Pleistocene glaciations. The alternative explanation suggested by Turnbull and Davies (2006) is that glacial cirques are in reality the scars of deep-seated landslides. In this way the problem of the slow growth in relationship to size is avoided. The authors cite as demonstrative example the Acheron rock avalanche in New Zealand. The mass failure, about 1,000 years old, has left a scar indistinguishable from those normally attributed to genuine glacial cirques. Indeed, if it had not been for the voluminous deposits proving the mass wasting nature of the Acheron, probably geomorphologists would consider it as a typical glacial cirque. Another indication in favor of this hypothesis is that cirques appear most often at the top of the slopes, exactly where the instability is supposed to occur.

One serious challenge to the model is the global orientation of cirques. Cirques in the Northern hemisphere are preferably directed to North, and in the southern hemisphere to South. This is easily explained in the standard model by the fact that both nivation and glacial erosions are faster for the slopes where the sun is weakest. The orientation effect is, conversely, difficult to reconcile with the landslide model. Another difficulty is that glacial cirques often appear in series (staircases), an uncommon feature in landslide scars. The lack of landslide deposits at the foot of most cirques is also problematic: it might be tentatively explained by removal by glaciers and river erosion (and perhaps mixing with morain deposits), but this seems partly an ad hoc explanation. Note also that owing to its high cohesion, rock rarely forms slumps, except perhaps for earthquake-induced failures. Nevertheless,

(continued)

Box 2.3 (continued)

although the hypothesis faces some objective difficulties to explain most glacial cirques, it is appealing in suggesting that at least some of the hollows previously attributed to cirques might in reality be the relicts of ancient catastrophes.

General references Chapter 2: Sidle and Ochiai ([2006](#)); Dikau et al. ([1996](#)); Turner and Schuster ([1996](#)), Duncan ([1996](#)), Dikau et al. ([1996](#)), Middleton and Wilcock ([1994](#)).

Introduction to the Physics of Landslides

Lecture notes on the dynamics of mass wasting

de Blasio, F.V.

2011, XV, 408 p., Hardcover

ISBN: 978-94-007-1121-1